

# Production of Niobium Nitride Via Nitrogen-Based Solid-Gas Reaction

Rayane Ricardo da Silva<sup>a\*</sup> , André Luís Lopes Moriyama<sup>b</sup>, Camila Pacelly Brandão de Araújo<sup>c</sup>,  
Yara Feliciano Gomes<sup>a</sup>, Carlson Pereira de Souza<sup>a,b</sup>

<sup>a</sup>Universidade Federal do Rio Grande do Norte, Departamento de Ciência e Engenharia de Materiais, Natal, RN, Brasil.

<sup>b</sup>Universidade Federal do Rio Grande do Norte, Departamento de Engenharia Química, Natal, RN, Brasil.

<sup>c</sup>Universidade Federal do Rio Grande do Norte, Escola de Ciências e Tecnologia, Natal, RN, Brasil.

Received: April 08, 2022; Revised: August 01, 2022; Accepted: August 04, 2022

Nanostructured niobium nitride was synthesized through a solid-gas reaction in an atmosphere of nitrogen and hydrogen using an oxalic niobium precursor. Crystal phases evolution throughout the reactive processes were evaluated using X-Ray Diffraction, reaction parameters modifications were performed in isotherm time, gas flow, and precursors' mass. It was verified the synthesis of a stable NbN material with a hexagonal structure under the following conditions: 1g of precursor, 300 min of isotherm at 1100 °C and, the gas flow of N<sub>2</sub> = 40% (v/v), and H<sub>2</sub> = 60% (v/v). The increase in gas phase flow and the decrease of solid load favored the process, and a pure and single-phase powder was obtained. This set indicates the importance of physical resistance in the fluid-particle interaction process. Under these conditions, the solid obtained had a crystallite size of 30 - 50 nm.

**Keywords:** *Solid-gas reaction, X-ray diffraction, hexagonal phase, niobium nitride.*

## 1. Introduction

The transition metal elements found in group V of the periodic table, of which niobium is part, when associated with other chemical elements, such as nitrides, develop chemical and physical properties of great technological interest, such as a high point melting, chemical stability, high hardness, good conductivity, and electrical resistance<sup>1</sup>. This means that many nitrides and carbides of niobium, tantalum, tungsten, and others, are increasingly studied as promising candidates for different industrial applications.

In particular, niobium nitrides present potential application in superconducting devices, such as in radiofrequency resonators, which make this specific metal a non-polluting and non-toxic alternative to conventional metals, lead for instance, among others.

It is known that materials production methods have an important impact on their properties and even on their form of crystallization<sup>2-6</sup>. Regarding the production of nitrides, researchers have established and studied different experimental procedures, such as reactive pulsed laser deposition (RPLD)<sup>7</sup>, synthesis via the urea route<sup>8</sup>, thermal diffusion of nitrogen<sup>9</sup>, solid-gas reaction at atmospheric pressure using ammonia as a nitrogen source<sup>10</sup>, and solid-gas reaction at high pressure<sup>11</sup>, among others. Among these methods, solid-gas has advantages when it comes to its ease of operation, low maintenance cost, and shorter processing time, in addition to enabling the control of the size and shape of the powder particles<sup>12</sup>.

However, most of the works that use this method are based on the use of ammonia as a nitrogen source, which is

more reactive than nitrogen gas but has disadvantages related to its high toxicity, and the use of niobium in the form of chloride or metal, which both have disadvantages related to the risks of handling the chloride and the requirement of another processing step to reduce it to metallic niobium. The use of niobium pentoxide as a metal source is limited due to its high chemical stability<sup>13</sup>.

Authors have studied different production routes of niobium oxalate compounds. More recently, it was realized that niobium oxalates have the potential of forming several compounds due to the high coordination capacity of niobium and the variety of forms of hexa or heptacoordinated groups with the (C<sub>2</sub>O<sub>4</sub>)<sup>2-</sup> ion<sup>14</sup>.

Niobium oxalate is an excellent material due to its low cost and does not suffer from disadvantages like halides or orthoniobates<sup>15</sup>. Niobium compounds present special properties, which are not present in compounds of the elements close by on the periodic table. Some properties of niobium oxalate such as thermal stability or decomposition mechanism are particularly important for the preparation of a good catalyst containing niobium.

Regarding the use of niobium oxalates as precursors for the production of other niobium compounds, the authors proved to be possible to use the niobium oxalate complex as a precursor for the production of its carbide at temperatures as low as 950 °C via solid-gas reaction<sup>16</sup>. The use of this precursor proved to be viable and favorable to the synthesis of niobium carbide due to its greater reactivity compared to niobium pentoxide. According to authors, copper-doped niobium carbide can be produced from the precursor niobium

\*e-mail: rayanebrasil@hotmail.com

oxalate with the addition of copper in the proportion of 5% and 10% at a temperature of 980 °C by the gas-solid method, forming a nanometer material of 20 nm size<sup>17</sup>.

Furthermore, authors report that the kinetic study related to the synthesis of niobium carbide from its pentoxide indicates that the increase in temperature increases the reaction rate, which is directly related to the reaction time<sup>18</sup>, while the initial mass produces the opposite effect, which is related to the diffusion of gases into and out of the dust layer<sup>19</sup>.

In this paper, we sought to investigate the formation of niobium nitride through a gas-solid reaction at atmospheric pressure using nitrogen gas as a source of this element and niobium oxalate as a source of the metal. For this purpose, a series of experiments were conducted and the effect of the synthesis parameters, such as reaction time, precursor mass, and gas mixture flow were evaluated, which allowed the establishment of important information regarding the phenomena associated with the production of nitride of niobium.

By the solid-gas reaction method used in this paper, it was possible to obtain a stable and pure niobium nitride phase with a hexagonal structure at the temperature of 1100 °C. To our knowledge, this is the first time that this type of study and result has been reported in the literature.

## 2. Materials and Methods

### 2.1. Precursor's synthesis

For the synthesis of the precursor tris(oxalate) ammonium oxyniobate hydrate  $(\text{NH}_4)_3\text{NbO}(\text{C}_2\text{O}_4)_3\text{H}_2\text{O}$  applied in solid-gas reactions, niobium pentoxide,  $\text{Nb}_2\text{O}_5$ , (99.9%, CBMM), potassium bisulfate,  $\text{KHSO}_4$  was used, (99.9%, SYNTH), ammonium oxalate,  $\text{C}_2\text{H}_8\text{N}_2\text{O}_4$ , (99.9%, SYNTH) and oxalic acid,  $\text{C}_2\text{H}_2\text{O}_4$ , (99.9%, SYNTH). A typical procedure for the production of said precursor follows the next steps<sup>20</sup>: niobium pentoxide and potassium bisulfate were mixed in a proportion of 1:7 by weight and heated to melting point in crucible platinum.

Then, it was ground, added water and heated for 40 min at 80 °C, and left to rest for 12 h. Next, the material was filtered and washed with hot water. Then, oxalic acid and ammonium oxalate 1:3 by weight with 150 ml of water were added and placed under continuous stirring at 65 °C with slow evaporation. The formed precipitate was dried in a muffle at 80 °C for 24 h.

### 2.2. Nitride synthesis

For the reactions aimed to study the production of niobium nitride through the solid-gas method at atmospheric pressure using gaseous nitrogen as a nitrogen source, the procedures listed below were followed. It began with the proper weighing of the hydrated ammonium oxyniobate precursor and its insertion into an alumina crucible with the following dimensions: 20 mm thick, 15 mm high, and 80 mm wide.

Then, the crucible was introduced into a fixed bed reactor coupled to a resistive furnace with temperature and heating rate control. Constructive details of the experimental apparatus can be seen in Figure 1. Before the start of the heating, argon gas (99.9%, Linde) was used to purge the reactor for 15 min to eliminate any gaseous impurities such as oxygen, monoxide and carbon dioxide, and water vapor. After purging, the flow of the gas mixture composed of  $\text{H}_2$  (99.9%, Linde) and  $\text{N}_2$  (99.9%, Linde) in the proportions of 60% (v/v) and 40% (v/v) respectively, was started.

Simultaneously, the reactor began to be heated at a rate of 10 °C / min to 1100 °C, the temperature at which the reaction is maintained for a certain period. Aiming to achieve the objectives of this study, the following reaction parameters were varied: soak time at a temperature of 1100 °C, the flow of the reaction gas mixture, and the initial mass of the precursor. Table 1 indicates the study ranges for these parameters. The values of the gas mixture composition as well as the heating rate of the reactor were optimized in preliminary studies carried out by the research team of our laboratory<sup>21</sup>.

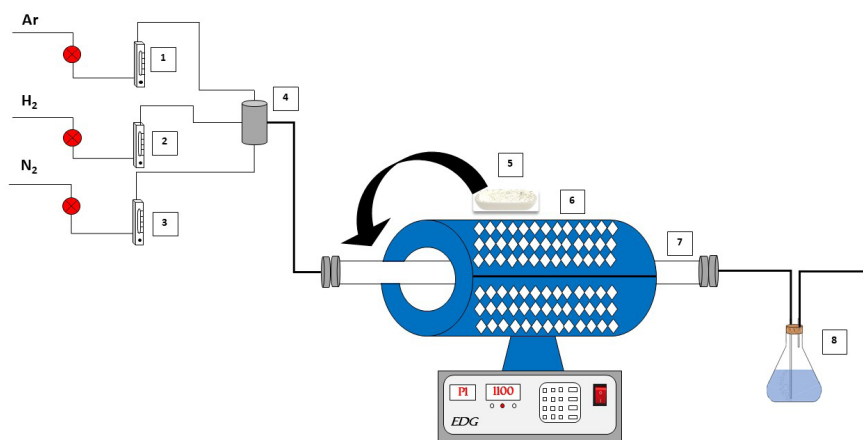


**Figure 1.** System: 1,2,3 - Gas flow controller, 4 - Gas mixer, 5 - Alumina crucible, 6 - Resistive furnace, 7 - fixed bed reactor, 8 - Bubble system.

**Table 1.** Reaction parameters of the experiments.

Parameters	Range
Isotherm time to 1100 °C (min)	0 – 360
Gas flow (L/h)	14.9 – 44.7
Precursor mass (g)	1 – 2

### 2.3. Characterization

The structure and composition of those required, according to the above parameters, were characterized by X-ray diffraction (XRD) (Shimadzu-7000 diffractometer), using CuK $\alpha$  radiation (30 mA, 30 kV,  $\lambda = 1.5418 \text{ \AA}$ ). To identify the phases, the crystalline ones use the PANalytical HighScore 3.0 software and the PDF (Powder Diffraction File) database. In possession of the X-ray diffraction data, the refinement of the structural parameters was also carried out by the Rietveld method using the GSAS software<sup>22</sup>. The VESTA software was also used to visualize the crystal structure<sup>23</sup>. The crystallite sizes of the samples were calculated from the mathematical models of Scherrer, Williamson-Hall, and Halder-Wagner-Langford. The reaction conversion rate was established based on these data and the measurement of the mass of the material after the reactions. In order to analyze the morphology of the materials, SEM images for all the samples obtained on a Carl Zeiss Auriga Field Emission Scanning Electron Microscope at 5.00 kV of working acceleration voltage and secondary electron (SE) detector. High-resolution transmission electron microscope (HRTEM) images were obtained using a JOEL-2010F with 200 kV of voltage and brightfield to obtain more detailed morphology information.

## 3. Results and Discussion

### 3.1. Effect of flow variation

By evaluating the effect of the flow rate in the reaction gas mixture on the synthesis process products, we observed the presence of the niobium oxide and niobium nitride phases, as can be seen in the diffractogram shown in Figure 2A, when the time at the isotherm of 1.100 °C is 180 min, flow rate of 14.9 L/h and reagent mass of 1g. After identifying the crystal structure of the phases present, it was noticed that it was the cubic NbN phase (PDF n°: 074-1218) and tetragonal NbO<sub>2</sub> (PDF n°: 082-1142).

Comparing the peak intensities of each phase with their standard structures, Figure 2, it can be seen that the most intense peaks for each phase present in Figure 2 are always associated with the main peaks of each crystal structure and that the other peaks respect the relative intensity present in the standard structures of each phase, which indicates that there are no crystal defects related to the grain growth process, being, therefore, isotropic processes from the crystallographic point of view. This fact leads to the conclusion that the reactions between the precursor and the nitrogen and hydrogen gases, all in the aforementioned proportions and quantities, provide an orderly growth of the crystallographic planes of each phase, which constitutes a thermodynamically favorable process for the production of cubic NbN and tetragonal NbO<sub>2</sub>.

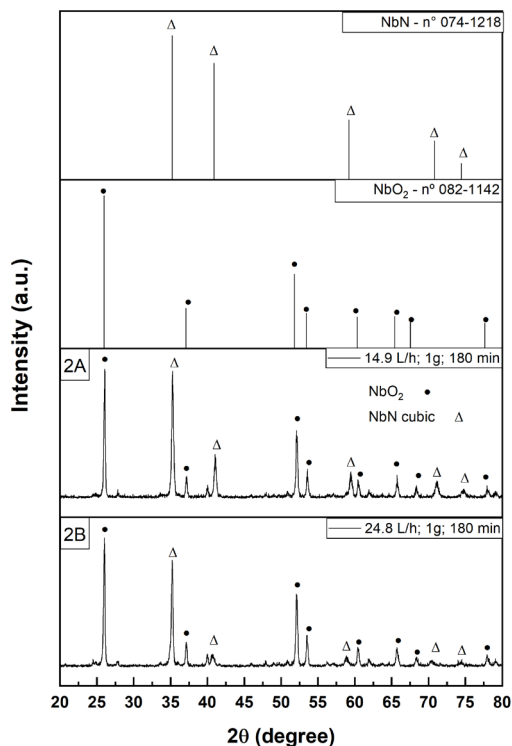
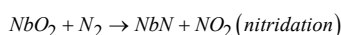


**Figure 2.** Diffractogram of the NbN samples in the synthesis conditions: precursor mass of 1 g and 180 min with a flow rate of 14.9 L/h (2A) and 24.8 L/h (2B).

When the flow rate of the reaction gases was increased to 24.8 L/h, a relative reduction was noted in the intensities of the niobium nitride phase peaks in the  $2\theta$  positions of 35° and 41°. It is known that the effect of gas-phase flow in gas-solid reactions is mainly expressed in the physical resistance to the transfer of molecules from the gas phase to the surface of the solid where the reaction takes place. Increasing the flow rate to a certain level tends to reduce the physical resistance to mass transfer, allowing us to know the predominant characteristics of chemical reactions, as well as reducing the residence time of the gas inside the reactor<sup>24</sup>. Based on the results of the literature, the stoichiometries of the niobium precursor transformation can be written as follows<sup>25-27</sup>:



### 3.2. Effect of precursor mass variation

In Figure 3 we present all the diffractograms of the powders produced by the proposed synthesis methodology under the conditions of 1 g and 2 g of precursor mass, 300 min isotherm, and total flow between 14.9 L/h and 44.7 L/h. Upon flow conditions of 14.9 L/h and precursor mass of 2 g (Figure 3A), we observed the presence of three distinct crystalline phases: niobium oxide (PDF n°: 082-1142), cubic niobium nitride (PDF n°: 074-1218), and hexagonal niobium nitride (PDF n°: 065-3417). The NbO<sub>2</sub> phase appears with its

characteristic peak at the 25° position and presents greater intensity when compared to both niobium nitride phases.

However, it is interesting to note that when the reaction time in the isotherm is increased to 300 min, the hexagonal niobium nitride phase is predominant (PDF n°: 065-3417), which points to a reaction mechanism where cubic niobium nitride acts as a precursor to hexagonal niobium nitride. As both have NbN stoichiometry, we conclude that the maintenance of cubic niobium nitride under the conditions tested makes it possible to reach higher levels of conversion of NbO<sub>2</sub> into the nitride and its recrystallization, starting from a cubic to hexagonal crystal structure.

These facts indicate that in 300 min we approach a thermodynamic equilibrium state and, simultaneously, that the most stable phase of niobium nitride is the hexagonal one. This information matches the comparison we made between the formation and crystallization energies of both materials. The greater the negative variation of Gibbs free energy, the more the process becomes irreversible and the compound formed becomes stable, not allowing the reaction to return to its origin<sup>28</sup>.

The modification of the initial mass of the solid precursor allows greater clarity in understanding the physicochemical phenomena related to the reaction between the niobium precursor and the nitrogen and hydrogen gases. We noted (see Figure 3B) that for an initial mass of 2 g of precursor, maintaining the same conditions as mentioned above of 300 min in the isotherm and flow rate of 24.8 L/h, there is, in the reaction product, the presence of NbO<sub>2</sub> phases, cubic and hexagonal NbN, which can be objectively explained by the same sequence of transformation of NbO<sub>2</sub> into NbN already described, plus the fact that the reaction progresses from the region of the solid in direct contact with the gas to the interior of the precursor mass. This process, from a

certain distance into the reaction layer, is governed to a greater extent by the diffusion of the gas than by its convection.

Therefore, we conclude that precursor particles in direct contact with the gaseous stream convert more rapidly to cubic NbN than interior particles and that in this progression there is still cubic NbN inside the solid when a part of the solid surface NbN has already been recrystallized in a hexagonal structure. The nature of the progression of the NbO<sub>2</sub> reaction to cubic NbN is typical of fixed bed reactors. Furthermore, the results show that the conditions tested to represent the limit from which thermodynamic equilibrium is reached are from the point of view of crystal structures.

By increasing the total flow to 24.8 L/h (Figure 3B), it is possible to observe the appearance of two other new peaks at positions 48°, 62°, and 65° that correspond to the hexagonal NbN, indicating that the increase in the total flow of the gas mixture favors the formation of this phase. As the total flow increased to 34.8 L/h (Figure 3C), there was a decrease in the intensity of niobium oxide and an increase in the intensity of the characteristic peak of hexagonal niobide at 2θ = 38°, confirming a higher concentration of this phase. In the synthesis process with the highest total flow rate of 44.7 L/h (Figure 3D), the predominant presence of the hexagonal NbN phase is observed, which indicates that the increase in the total flow favors the formation of this phase. In this condition, the conversion of NbO<sub>2</sub> to hexagonal NbN is greater than 95%. The lattice parameters and position were estimated using the Rietveld refinement method and were analyzed using the Structure Analysis System (GSAS) program with an EXPGUI graphical interface program.

In Figure 3E with an isotherm of 300 min and precursor mass of 1 g, the peaks are attributed to the hexagonal structure of NbN, except for the peak at 25° which corresponds to NbO<sub>2</sub>. It is still possible to identify the presence of niobium

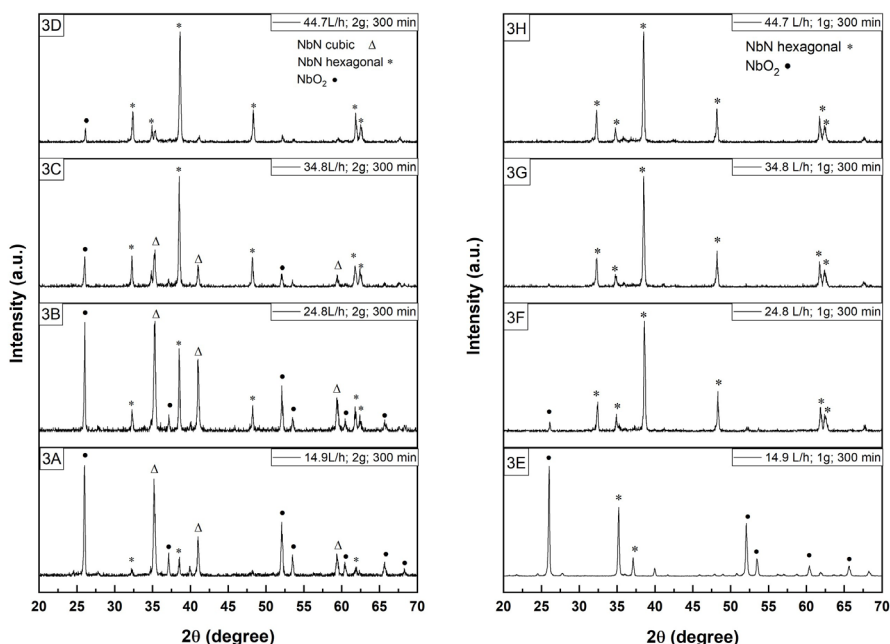


**Figure 3.** XRD of the NbN samples in the total flow range of 14.9 L/h to 44.7 L/h with 300 min of isotherm and precursor mass of 2 g (3A, 3B, 3C, 3D) and 1 g (3E, 3F, 3G, 3H), respectively.

oxide represented by the lowest intensity peak at  $2\theta = 25^\circ$ . With the increase of the total flow to levels between 34.8 L/h (Figure 3G) and 44.7 L/h (Figure 3H), it was evident that all peaks correspond only to the hexagonal phase of niobium nitride, demonstrating a stable structure for these synthesis conditions. Therefore, the increase in the total flow rate of the reaction system and the smaller amount of precursor sample are factors that influence the formation of the product with the absence of secondary phases.

This paper observed that increasing the total flow rate of the gas mixture influences the reaction rate and improves the nitriding process, favoring the formation of the hexagonal phase, which is found at a temperature lower than that of the cubic phase according to the Nb-N diagram<sup>29</sup>. The different proportions of the nitride cubic and hexagonal were found and analyzed by the program GSAS according to the parameters studied in this paper.

### 3.3. Effect of isotherm time variation

The duration of the reaction time in the isotherm brings further clarifications about the studied system. Figure 4 shows the structural evolution of samples prepared for different processing times from 0 to 360 min, using the precursor mass of 1 g under a total gas flow of 44.7 L/h. In the reaction time from 0 to 120 min, only the presence of peaks of niobium oxide and cubic niobium nitride can be observed, maintaining constancy in the similarity to the x-ray diffractograms. In the 180 min isotherm, the  $\text{NbO}_2$  phase disappears and it is possible to observe the beginning of the evolution of NbN

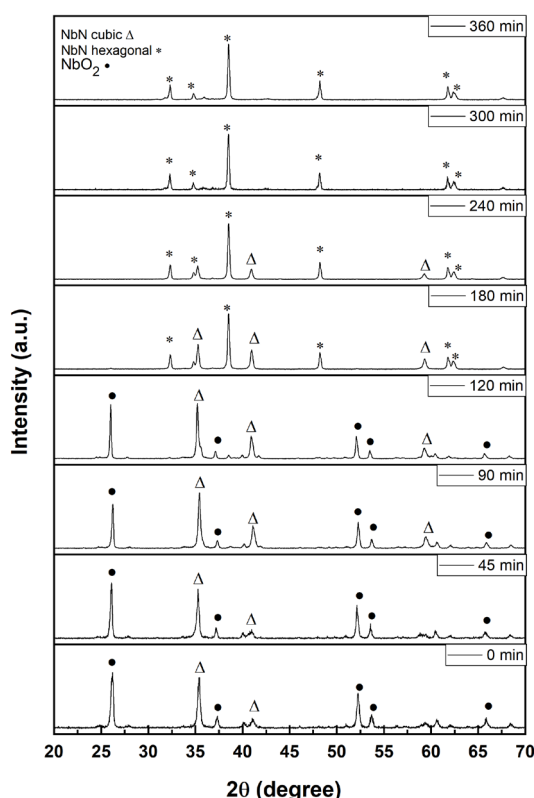


**Figure 4.** XRD of the NbN samples in the time from 0 to 360 min, precursor mass of 1 g, and total flow rate of 44.7 L/h.

with hexagonal structure at positions  $32^\circ$ ,  $38^\circ$ ,  $48^\circ$ , and  $62^\circ$  and  $65^\circ$ , with its characteristic peak at  $2\theta = 38^\circ$  becoming the most intense peak.

With the increase of time to 240 min, the hexagonal NbN phase is predominant in the diffraction pattern, and it can be seen that this phase becomes stable<sup>30,31</sup>. It is important to note that the diffractograms obtained on the powders produced with isotherm times of 180, 240, 300, and 360 min showed similarities regarding the present crystal structure. Thus, it is possible to observe a significant effect of the time interval in the reaction system for the formation of monophasic NbN and we found out that the minimum time required for its production is 300 min.

### 3.4. Evaluation of crystallite powder size

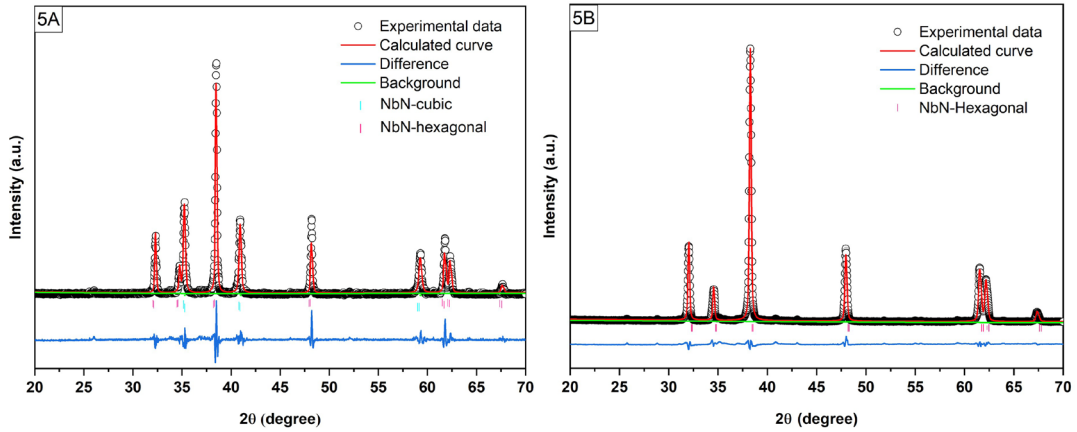
Figure 5 shows the results of the Rietveld method refinement performed in the GSAS software. Figure 5A shows the X-ray diffractogram for the reaction sample with isotherm of 180 min using 1 g of precursor mass and flow rate of 44.7 L/h, containing phases cubic NbN and hexagonal NbN. The results obtained by refinement by the Rietveld method were  $R_{wp}$  of 23.76% and  $\chi^2$  of 3.15. Figure 5B shows the results for the sample produced with a reaction duration of 300 min using 1 g of precursor mass and flow 44.7 L/h, which has pure hexagonal NbN. The factors  $R_{wp}$  and  $\chi^2$  are related to the convergence of the refinement and an  $R_{wp}$  of 11.38% and  $\chi^2$  of 9.28 were obtained, respectively. With the values obtained from these refinements, it was possible to verify a satisfactory fit between the XRD pattern of the samples and the pattern refined by Rietveld.

Table 2 shows the values obtained through the refinement with the parameters found in the standard chart of the reaction of the 180 min, 1 g precursor mass, flow 44.7 L/h with the presence of the cubic and hexagonal phases. The hexagonal NbN structure, analyzing the results of the refinement, an contraction of the crystal structure around 0.35% of the lattice parameters "a" and "b" are observed, and a contraction of the structure of 0.18% of the parameter "c" in comparison with the standard data (PDF n°: 065-3417). The data obtained in the refinement for the sample of cubic NbN structure, show that the network parameters had a contraction of 0.04% compared to the standard chart (PDF n°: 075-1218).

Figure 6 shows a representation of the unit cells obtained by Vesta software. The possible to observe the phases cubic and hexagonal organization structure in agreement with the refinements in Figure 5. Where the niobium atoms are represented in blue color and the nitrogen atoms in orange color. Figure 6A shows the structure of NbN with cubic and hexagonal phases, as obtained through the X-ray diffractogram and Rietveld refinement of Figure 5A. The cubic phase has a space group Fm-3m and number 225 and the hexagonal phase has a space group P63/mmc and number 194. Figure 6B shows the structure of the pure structure of the NbN with the hexagonal phase based on the results of the Rietveld refinement of Figure 5B and proves the same space group P63/mmc.

The crystallite size was calculated using the XRD using the Debye-Scherrer equation (1):

$$D = \frac{k\lambda}{\beta \cos\theta} \quad (1)$$



**Figure 5.** The NbN diffraction pattern obtained by the Rietveld method in the 1g precursor mass, 44.7 L/h and time of 180 min (A) e 300 min (B).

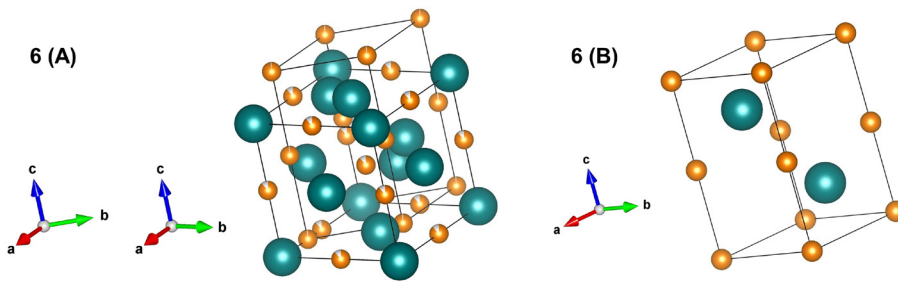


**Figure 6.** Projection of the unit cell of the hexagonal structure of the NbN.

**Table 2.** Values structural parameters of the NbN from the data obtained in the refinement of the 180 min reaction under the conditions of 1g of precursor mass and 44.7 L/h and the values from the pattern.

Sample NbN	Crystalline structure	a (Å)	b (Å)	c (Å)	V (Å <sup>3</sup> )
Refinement	Hexagonal	2.9786	2.9786	5.5386	42.55
(PDF n°: 065-3417)	Hexagonal	2.9680	2.9680	5.5490	42.33
Refinement	Cubic	4.4079	4.4079	4.4079	85.64
(PDF n°: 075-1218)	Cubic	4.4100	4.4100	4.4100	85.77

Where  $D$  is the crystallite diameter,  $\lambda$  is the wavelength (1.5406 Å),  $\beta$  is the width at half-height of the diffraction peak (FWHM) and  $\theta$  is the Bragg angle. Calculations are based on the magnification of the peaks of the diffraction patterns. In Figure 4, in the time interval from 180 min to 360 min, we observe the most intense peak at  $2\theta = 38^\circ$  which corresponds to the 101 direction, where we can relate the crystallite size with the integrated area under the peak. As shown in Figure 7, as the peak area reduction occurred as a function of the processing time, the crystallite size increased, ranging from 38 to 40 nm according to the Scherrer model equation. Table 3 shows the estimated values of the crystallite sizes using Equation 1 by the normal and integral peak width method. We verified that the values obtained by the normal method are around 70% higher when compared to the integral method.

The Williamson-Hall (Equation 2) and Halder-Wagner-Langford (Equation 3) mathematical models take into account the micro deformation ( $\varepsilon$ ) that exists in the structures of the

**Table 3.** Crystallite size by Scherrer method.

Reaction time (min)	D Scherrer normal (nm)	D Scherrer integral (nm)
180	53.40	39.42
240	52.50	39
300	53.71	39.21
360	54.34	40.01

materials and estimate the crystallite size by checking the slopes and intersections on the x-axis of the straight-line equations.

$$\frac{\beta}{\lambda} \cos\theta - \frac{K}{D} + \frac{4\varepsilon}{\lambda} \sin\theta \quad (2)$$

$$\left( \frac{\beta \cos\theta}{2 \sin\theta} \right)^2 = \frac{1}{D} \frac{\beta \cos\theta}{(2 \sin\theta)^2} + \left( \frac{\varepsilon}{2} \right)^2 \quad (3)$$

Table 4 shows the values obtained for the desired variables, which are crystallite sizes, correlation coefficients ( $R^2$ ), and micro strain ( $\epsilon$ ) after adjusting the mathematical profile from the experimental data. By analyzing the results presented for the time intervals from 180 min to 360 min, it can be seen that they satisfy the Halder-Wagner-Langford (HWL) method, as the  $R^2$  correlation coefficients are  $> 0.95$ , indicating a good fit between the data and the model.

Also, it was possible to observe that using the normal method presented a better linearization. The smaller values of  $R^2$  in the 180 min time can be explained by the fact of the presence of two phases of niobium nitride, while the coexistence of different structures can result in changes in the crystal lattice. Thus, when only the hexagonal NbN phase at the 300 and 360 min times was obtained, the correlation

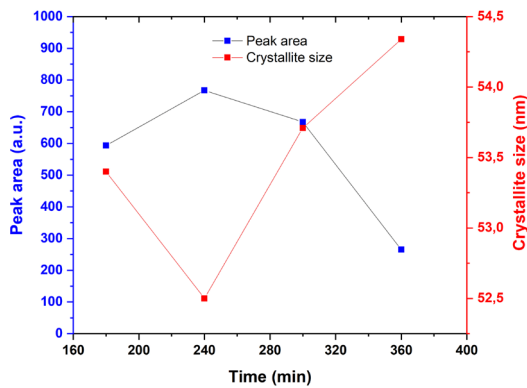


**Figure 7.** NbN crystallite size as a function of the synthesis processing time.

becomes more reliable. From the calculations performed it is verified that the crystallite sizes present a significant variability and lack of homogeneity, but with sizes smaller than 42 nm in all cases.

The morphologies of NbN nanoparticles were observed by SEM/FEG. The morphologies of the NbN obtained after synthesis with 300 min at 44.7 L/h and 1 g of precursor are shown in Figures 8A and 8B. It was possible to identify in the images clusters of spherical particles of hexagonal NbN of different sizes, representing the same behavior in all the samples.

Figure 9 represents the image of NbN morphology by HRTEM measurements. Image 9 (A) shows the NbN particles with the cubic phase and the hexagonal phase obtained after the treatment condition at 180 min, 1 g of precursor mass and a flow rate of 44.7 L/h. The image reveals that it has small parts of nanoparticles in the cubic phase, while the rest are particles in hexagonal shape. In order to obtain the most detailed structure and composition of NbN, various image HRTEM was performed. Figure 9B shows the distance between the planes (111) was 0.25 nm from the cubic phase of NbN, according to the distance listed in the literature<sup>31</sup> and in the pattern (PDF n°: 075-1218). As shown in Figure 9C, the image shows the distance interplanar was 0.13 nm oriented in the plane (200) and coincides with the pattern (PDF n°: 065-3417). Figure 9D represents the image of pure NbN nanocrystals under conditions of 300 min, 1 g of precursor mass, and a flow of 44.7 L/h. The image shows the NbN cluster and it is possible to observe only the structure of the hexagonal phase. Figure 9E shows the single-phase HRTEM image of the NbN nanocrystal and the measured distance between the plane (101) was 0.23 nm, according to the pattern (PDF n°: 065-3417).

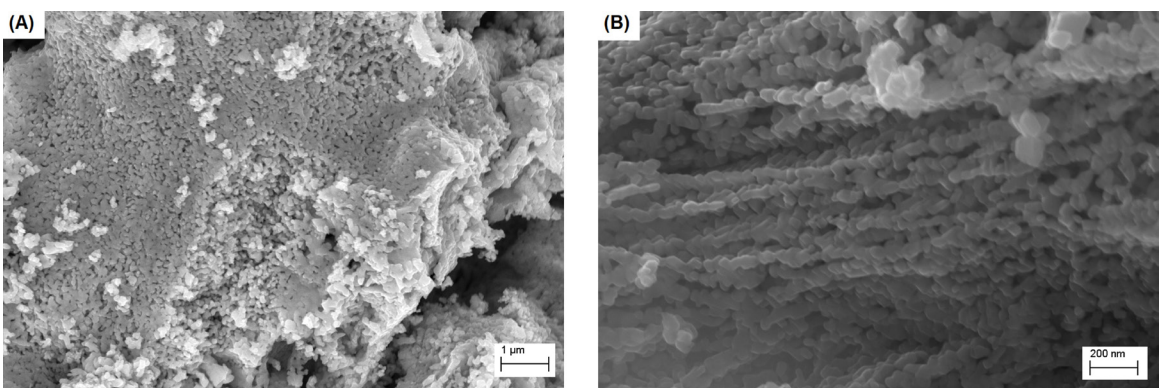


**Figure 8.** SEM/FEG images of the as-prepared NbN hexagonal in the conditions of 300 min to flow rate of 44.7 L/h, and precursor mass of 1 g.

**Table 4.** Crystallite size using the Halder-Wagner-Langford and Williamson-Hall methods.

Time (min)	HWL Normal			HWL Integral			WH Normal			WH Integral		
	D (nm)	$\epsilon$	$R^2$	D (nm)	$\epsilon$	$R^2$	D (nm)	$\epsilon$	$R^2$	D (nm)	$\epsilon$	$R^2$
180	50.38	0.0030	0.7899	34.25	0.0073	0.7486	57.89	0.0005	0.0617	49.99	0.3024	0.2695
240	37	0.0034	0.8222	22.32	0.0058	0.7479	49.74	0.0004	0.0180	45.31	0.3722	0.1206
300	38.80	0.0043	0.9748	23.49	0.0009	0.9320	35.45	-0.0008	0.4675	28.34	-0.0082	0.0003
360	41.94	0.0036	0.9679	27.32	0.0045	0.9625	39.08	-0.0006	0.3933	31.03	0.0233	0.0069

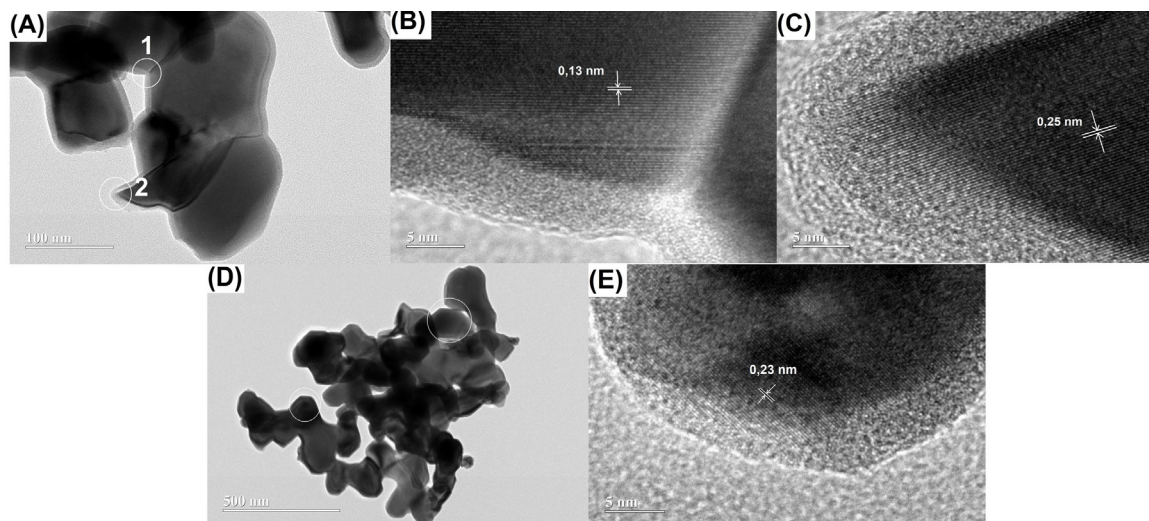


**Figure 9.** HRTEM of the NbN: (A) hexagonal and cubic phases, (B) hexagonal phase (area 1), (C) cubic phase (area 2) and (D, E) hexagonal phase pure.

## 4. Conclusions

In this paper, the study of the production of pure niobium nitride through an innovative gas-solid reaction route, green by acting at atmospheric pressure, and of the exceptionally low toxicity by using nitrogen gas as raw material. The conditions studied allowed us to understand the physicochemical phenomena that interfere in the production of niobium nitride both from a reactional and a crystallographic point of view. From the observation and understanding of these phenomena, we scientifically point out the factors that lead to the effectiveness of the proposed method, which, as far as we know, have never been reported and used for this purpose.

Through the analysis of X-ray diffractograms, we found out that the combination of the total flow of the gas mixture between the levels of 34.8 and 44.7 L/h and the reduction of the initial precursor mass optimized the synthesis conditions regarding the elimination of the intermediate phase  $\text{NbO}_2$ . The use of reaction duration times in the isotherm equal to or greater than 300 min leads to the production of the hexagonal NbN phase, which proved to be the stable phase from the thermodynamic point of view.

In shorter times, there is the presence of the cubic NbN phase, which recrystallizes in hexagonal. The evaluation of the crystallite size by the mathematical models of Scherrer and Halder-Wagner-Langford showed us the existence of particles between 30 and 50 nm in average diameter. With this work, we conclude that the proposed production route can produce nanometric hexagonal NbN under green and non-toxic conditions, and we present the explanations for this.

## 5. Acknowledgments

The authors acknowledge CAPES/Brazil (Finance Code 001) for their financial support and the post graduate program in Materials Science and Engineering (PPGCEM).

## 6. References

1. Yeh CL, Chuang HC. Experimental studies on self-propagating combustion synthesis of niobium nitride. *Ceram Int.* 2004;30(5):733-43.
2. Lengauer W, Bohn M, Wollein B, Lisak K. Phase reactions in the Nb-N system below 1400°C. *Acta Mater.* 2000;48(10):2633-8.
3. Ma J, Du Y, Qian Y. Low-temperature synthesis of nanocrystalline niobium nitride via a benzene-thermal route. *J Alloys Compd.* 2005;389(389):296-8.
4. Ufuktepe Y, Farha AH, Kimura S, Hajiri T, Karadağ F, Al Mamun MA, et al. Structural, electronic, and mechanical properties of niobium nitride prepared by thermal diffusion in nitrogen. *Mater Chem Phys.* 2013;141(1):393-400.
5. Buscaglia V, Caracciolo F, Ferretti M, Minguzzi M, Musenich R. Effect of pressure on the composition and superconducting  $T_c$  value of NbN prepared by combustion synthesis. *J Alloys Compd.* 1998;266(1-2):201-6.
6. Silva AGP, Souza CP, Gomes UU, Medeiros FFP, Ciaravino C, Roubin M. Low temperature synthesized NbC as grain growth inhibitor for WC-Co composites. *Mater Sci Eng A.* 2000;293(1):242-6.
7. Krishnan R, David C, Ajikumar PK, Dash S, Tyagi AK, Jayaram V, et al. Reactive pulsed laser deposition and characterization of niobium nitride thin films. *Surf Coat Tech.* 2011;206:1196.
8. Gomathi A, Rao CNR. Nanostructures of the binary nitrides, BN, TiN, and NbN, prepared by the urea-route. *Mater Res Bull.* 2006;41(5):941-7.
9. Farha AH, Ozkendir OM, Elsayed-Ali HE, Myneni G, Ufuktepe Y. The effect of heat treatment on structural and electronic properties of niobium nitride prepared by a thermal diffusion method. *Surf Coat Tech.* 2017;309:54-8.
10. Li Y, Gao L. Synthesis and characterization of nanocrystalline niobium nitride powders. *J Am Ceram Soc.* 2003;7(186732):1205-7.
11. Joguet M, Lengauer W, Bohn M, Bauer J. High-temperature reactive phase formation in the Nb-N system. *J Alloys Compd.* 1998;269(1-2):233-7.
12. Medeiros FFP, Oliveira SA, Souza CP, Silva AGP, Gomes UU, Souza JF. Synthesis of tungsten carbide through gas-solid reaction at low temperatures. *Mater Sci Eng A.* 2001;315(1-2):58-62.
13. Fontes FAO, Gomes KKP, Medeiros FFP, Souza CP, Sousa JF, Gomes UU. Synthesis of niobium carbide from ammonium

- niobium (V) oxalate precursor at low temperature in rotating cylinder reactor. *Mater Sci Forum*. 2005;498:747.
14. Papulovskiy E, Kirik SD, Khabibulin DF, Shubin AA, Bondareva VM, Samoilo AS, et al. Condensation of ammonium niobium oxalate studied by NMR crystallography and X-ray powder diffraction. *Catal Today*. 2020;354:26-35.
  15. Su TT, Zhai YC, Jiang H, Gong H. Studies on the thermal decomposition kinetics and mechanism of ammonium niobium oxalate. *J Therm Anal Calorim*. 2009;98(2):449-55.
  16. Medeiros FFP, Silva AGP, Souza CP. Synthesis of niobium carbide at low temperature and its use in hardmetal. *Powder Technol*. 2002;126(2):155-60.
  17. Souto MVM, Araujo CPB, Lima MJS, Borges FMM, Gomes UU, Souza CP. Synthesis and characterization of niobium carbide with copper addition obtained via gas solid reaction. *Mater Res*. 2018;21(3).
  18. Fontes FAO, Sousa JF, Souza CP, Benachour M, Bezerra MBD. Avaliation of gas phase kinetics of the carburization and deactivation reactions aimed to produce NbC. *Chem Eng J*. 2012;184:303-7.
  19. Medeiros FFP, Silva AGP, Souza CP, Gomes UU. Carburization of ammonium paratungstate by methane : the influence of reaction parameters. *Int J Refract Met Hard Mater*. 2009;27(1):43-7.
  20. Medeiros FFP, Moura MFV, Silva AGP, Souza CP, Gomes KKP, Gomes UU. The thermal decomposition of monohydrated ammonium oxotris (oxalate) niobate. *Braz J Chem Eng*. 2006;23(04):531-8.
  21. Silva AL, Souza RR, Moriyama CP. **BR 870180016744**. 2018.
  22. Toby BH. EXPGUI, a graphical user interface for GSAS. *J Appl Cryst*. 2001;34(2):210-3.
  23. Momma FIK. VESTA 3 para visualização tridimensional de cristal, dados volumétricos e morfológicos. *J Appl Cryst*. 2011;44:1272.
  24. Angelkort C, Lewalter H, Warbichler P, Hofer F, Bock W, Kolbesen BO. Formation of niobium nitride by rapid thermal processing. *Spectrochim Acta A Mol Biomol Spectrosc*. 2001;57(10):2077-89.
  25. Kim HS, Bugli G, Djéga-Mariadassou G. Preparation and characterization of niobium carbide and carbonitride. *J Solid State Chem*. 1999;142(1):100-7.
  26. Souto MVM, Lima MJS, Barbosa CM, Gomes UU, Souza CP, Araújo CPB. Synthesis and characterization of CuNb<sub>2</sub>O<sub>6</sub> from an oxalic precursor via solid state reaction. *Mater Res*. 2016;19(4):865-9.
  27. Teixeira da Silva VLS, Schmal M, Ko EI, Oyama ST. Synthesis of niobium carbide from niobium oxide aerogels. *Chem Mater*. 1995;7(1):179-84.
  28. Zhitomirsky V, Grimberg I, Rapoport L, Travitzky NA, Boxman RL, Goldsmith S, et al. Structure and mechanical properties of vacuum arc-deposited NbN coatings. *Thin Solid Films*. 1998;326(1-2):134-42.
  29. Dhakal P. Nitrogen doping and infusion in SRF cavities: a review. *Phys. Open*. 2020;5(June):100034.
  30. Cetinkaya S, Eroglu S. Thermodynamic analysis and synthesis of fine WC powder in the WO<sub>3</sub>-CH<sub>4</sub>-H<sub>2</sub> system using excessive CH<sub>4</sub>. *JOM*. 2017;69(10):2003-8.
  31. Lima MJS, Silva FES, Souto MVM, Araújo KFG, Menezes RAC, Filgueira M, et al. Effect of synthesis parameters on the crystallite size of WC-Ni composite powders obtained by gas-solid reaction. *Ceram Int*. 2021;47(16):23480-7.